January 26, 2010 | vol. 107 | no. 4 | pp. 1255–1690

PNAS

Proceedings of the National Academy of Sciences of the United States of America

www.pnas.org

Remarkable deformability of red blood cells

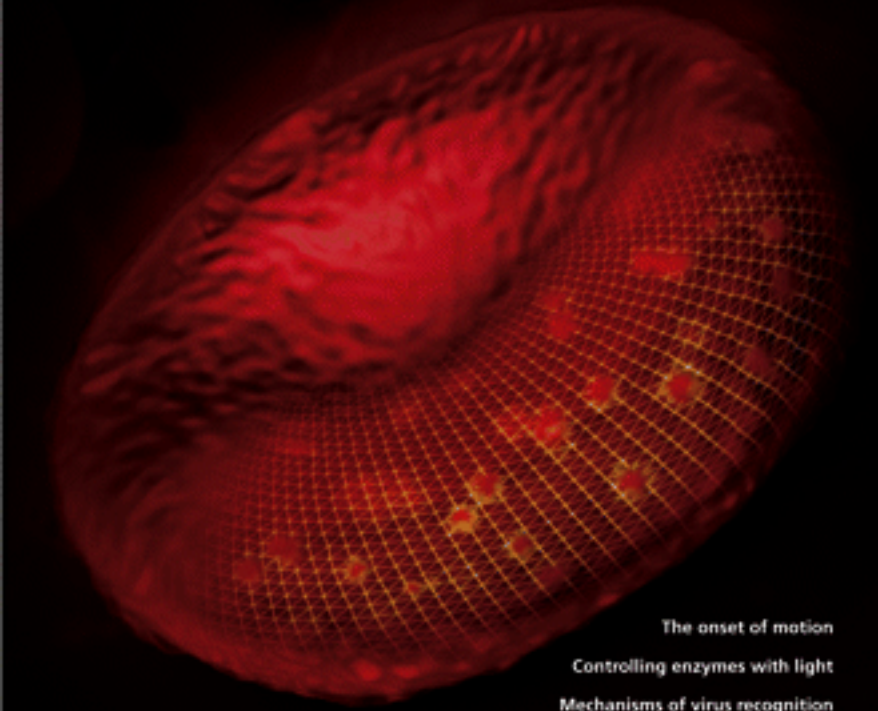

The onset of motion

Controlling enzymes with light

Mechanisms of virus recognition

A link between Alzheimer's and Down Syndrome

Metabolic remodeling of the human red blood cell membrane

YongKeun Park[a,b], Catherine A. Best[c], Thorsten Auth[d,e], Nir S. Gov[f], Samuel A. Safran[e], Gabriel Popescu[g], Subra Suresh[b,h,1], and Michael S. Feld[a,1]

[a]G. R. Harrison Spectroscopy Laboratory and [h]School of Engineering, Massachusetts Institute of Technology, Cambridge, MA 02139; [b]Harvard-Massachusetts Institute of Technology Division of Health Science and Technology, Massachusetts Institute of Technology, Cambridge, MA 02139; [c]College of Medicine and [g]Quantitative Light Imaging Laboratory, Department of Electrical and Computer Engineering, Beckman Institute for Advanced Science & Technology University of Illinois at Urbana-Champaign, Urbana, IL 61801; [d]Forschungszentrum Jülich, Institute for Solid State Research, 52425 Jülich, Germany; and [e]Department of Materials and Interfaces and [f]Department of Chemical Physics, Weizmann Institute of Science, P.O. Box. 26, Rehovot 76100, Israel

Edited by Zdeněk P. Bažant, Northwestern University, Evanston, IL, and approved November 25, 2009 (received for review September 18, 2009)

The remarkable deformability of the human red blood cell (RBC) results from the coupled dynamic response of the phospholipid bilayer and the spectrin molecular network. Here we present quantitative connections between spectrin morphology and membrane fluctuations of human RBCs by using dynamic full-field laser interferometry techniques. We present conclusive evidence that the presence of adenosine 5′-triphosphate (ATP) facilitates non-equilibrium dynamic fluctuations in the RBC membrane that are highly correlated with the biconcave shape of RBCs. Spatial analysis of the fluctuations reveals that these non-equilibrium membrane vibrations are enhanced at the scale of spectrin mesh size. Our results indicate that the dynamic remodeling of the coupled membranes powered by ATP results in non-equilibrium membrane fluctuations manifesting from both metabolic and thermal energies and also maintains the biconcave shape of RBCs.

ATP | imaging technique | membrane fluctuation | RBC | spectrin

As they travel through small blood vessels and organs, RBCs undergo repeated severe deformation. The coupling and interactions between the phospholipid bilayer and the spectrin network govern the deformability of RBCs (1). The fluid-like lipid bilayer is coupled to the two-dimensional spectrin network that comprises an approximately hexagonal lattice via protein junctional complexes. The RBC membrane is remarkably soft and elastic, and thus exhibits fluctuations with amplitudes of the order of tens of nanometers. The dynamics of the RBC membrane is strongly related to the membrane structure and mechanical properties and has been explored extensively (2–6). However, experimental results available to date on RBC membrane fluctuations have provided only limited information on select regions of the cell membrane with limited spatial and/or temporal resolution (7–9). No full-field measurements of membrane fluctuations in the entire RBC arising in response to well-controlled metabolic activity have been made so far and, consequently, different techniques have led to different interpretations of the mechanistic origins of dynamic RBC membrane fluctuations with and without metabolic activity (7–9).

The RBC membrane is not a static but a metabolically regulated active structure. It is known that biochemical energy controls its static and dynamic characteristics. The presence of ATP is not only crucial in maintaining the biconcave shape of the RBC membrane (10), but was also shown to increase the dynamic membrane fluctuations (7, 9). However, the regulatory mechanism of ATP in RBC membranes still remains elusive. Furthermore, these static and dynamic effects of ATP on RBC membrane fluctuations have hitherto been regarded as separate phenomena and have never been explored simultaneously.

Here, we present dynamic, full-field, and quantitative measurements of ATP effects on RBC membrane morphology and fluctuations. We show that in the presence of ATP, the RBC membrane fluctuations have a non-equilibrium, metabolic component in addition to a thermal one. The characteristics of this metabolically driven dynamics are observed only in the convex regions of the RBC membrane, with a periodic spacing on the order of the spectrin molecular network length scale. We demonstrate through systematic experiments that the metabolic energy of ATP dynamically remodels the coupling between a lipid layer and a spectrin network that governs both the biconcave shape and non-equilibrium fluctuations in RBC membranes. Through these observations, we also rationalize the origins of differing mechanistic interpretations of RBC membrane fluctuations (commonly referred to as "flickering") specifically in the context of the role of ATP.

Results and Discussions

ATP Effect on the RBC Morphology. We first address the effects of ATP on the morphology of RBC membranes. RBC samples were prepared under four different conditions: healthy RBCs, RBCs with irreversibly depleted ATP, metabolically depleted ATP, and repleted ATP groups. After collection, a group of healthy RBCs was minimally prepared (see *Materials and Methods*). For RBCs in the irreversibly depleted ATP group, the cytoplasmic pool of ATP was depleted by inosine and iodoacetamide. For the metabolically depleted ATP group, healthy RBCs were incubated in a glucose-free medium for 24 h. For RBCs in the ATP-repleted group, cytoplasmic ATP was first metabolically depleted and then regenerated through the addition of D-glucose. To quantitatively measure the cell thickness map, we employed Diffraction Phase Microscopy (DPM) (11, 12). By extracting the optical path-length shifts produced across the cell, we measured the cell thickness with nanometer sensitivity and millisecond temporal resolution. From the measured cell thickness profiles at a given time t, $h(x,y,t)$, we calculated time-averaged heights $\langle h(x,y)\rangle$ (Fig. 1*A–D*). We observed the characteristic biconcave shape for healthy RBCs. When ATP was depleted for both the irreversibly and the metabolically depleted groups, we observed loss of biconcave shape and echinocyte shape transformation. Reintroducing ATP resulted in the recovery of biconcave shape. This shows that ATP is crucial to maintaining the biconcave shape of RBCs (13).

Author contributions: Y.P., C.A.B., G.P., and M.S.F. designed research; Y.P. performed research; Y.P., T.A., N.S.G., S.A.S., and G.P. analyzed data; Y.P., G.P., S.S., and M.S.F. wrote the paper; and C.A.B. and S.S. contributed new reagents/analytic tools.

The authors declare no conflict of interest.

This article is a PNAS Direct Submission.

Freely available online through the PNAS open access option.

[1]To whom correspondence may be addressed. E-mails: ssuresh@mit.edu or msfeld@mit.edu

This article contains supporting information online at www.pnas.org/cgi/content/full/0910785107/DCSupplemental.

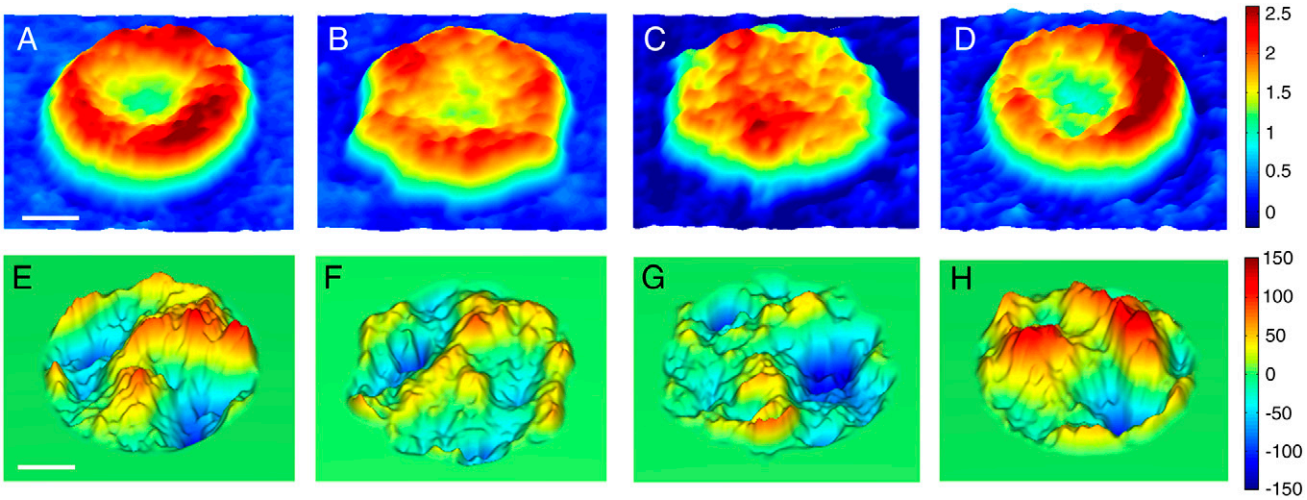

Fig. 1. Effects of ATP on morphology and dynamic fluctuation in RBC membrane. Topography of a healthy RBC, (*A*) of an ATP-depleted RBC (irreversible-ATP group), (*B*) of an ATP-depleted RBC (metabolic-ATP group), (*C*, and of a RBC with recovered ATP level (+ATP group), (*D*) resp. (*E–H*) Instantaneous displacement maps of membrane fluctuation in the Fig. 1*A–D*, resp. The scale bar is 2 μm. The colorbar scales are in μm and nm, resp.

Enhanced Membrane Fluctuations in the Presence of ATP. To probe dynamic membrane fluctuations, we analyzed the membrane displacement map by subtracting the averaged shape from the cell thickness map, $\Delta h(x,y,t) = h(x,y,t) - \langle h(x,y)\rangle$ (Fig. 1*E–H* and *Supporting Information* Movies S1–4). Compared to healthy RBCs, the fluctuation amplitudes were decreased in both ATP-depleted groups. Reintroducing ATP, however, increased the fluctuation amplitudes to healthy RBC levels. We calculated the RMS displacement of membrane fluctuations, $\sqrt{\langle \Delta h^2 \rangle}$, that covers the entire cell area for 2 s at 120 frame/s (Fig. 2). The RMS displacement of healthy RBCs is 41.5 ± 5.7 nm. Fluctuations significantly decreased to 32.0 ± 7.8 nm and 33.4 ± 8.7 nm in both the irreversibly and metabolically ATP-depleted groups, respectively. However, the fluctuations in the ATP-repleted group returned to the level of healthy RBCs (48.4 ± 10.2 nm). This is in agreement with an earlier report using the point measurement technique (9, 10).

ATP Results in Non-equilibrium Dynamics for Membrane Fluctuations. We showed that the membrane fluctuations indeed decrease in the absence of ATP, which is consistent with the previous results by using point measurement techniques (7, 9). However, this result does not yet answer the question of whether ATP drives "active," non-equilibrium dynamics or simply modifies membrane elastic properties. Of course, the two different situations can give rise to fundamentally different dynamics: (*i*) out-of-equilibrium fluctuations or (*ii*) equilibrium Gaussian fluctuations. To answer this question, we calculated the non-Gaussian parameter, κ, for the membrane fluctuations (Fig. 3*A–D*). Theoretically, $\kappa = 2$ for purely thermally-driven Gaussian motion and κ increases above two for active non-equilibrium dynamics (14). For healthy RBCs, the average value of κ was 2.8, which shows that membrane fluctuations contain non-equilibrium dynamic components, particularly on short length and time scales ($q > 5$ rad/μm and $\Delta t < 0.5$ s). With depletion of ATP, κ decreased to two, as expected in purely thermally-driven dynamics (the average values of κ were 2.06 and 2.19 for the irreversibly depleted and metabolically depleted ATP groups, resp.). Reintroducing ATP increased κ to healthy RBC levels (average value $\kappa = 2.98$). Our data clearly proves that active, metabolic energy from ATP contributes an enhancement in RMS displacements by 44.9%. This measured value is lower than predicted by a theoretical model where an increase of at least 100% was expected (14). However, it can be explained by recognizing that the ATP effect is more significant at large q-values, comparable with the size of the spectrin network (15). For example, the ATP-mediated RMS displacement at $q = 17 \pm 0.5$ rad/μm showed an increase of 143% compared with the thermal components. Thus, in our overall assessment that includes all spatial frequencies, ATP enhancement is likely to be underestimated.

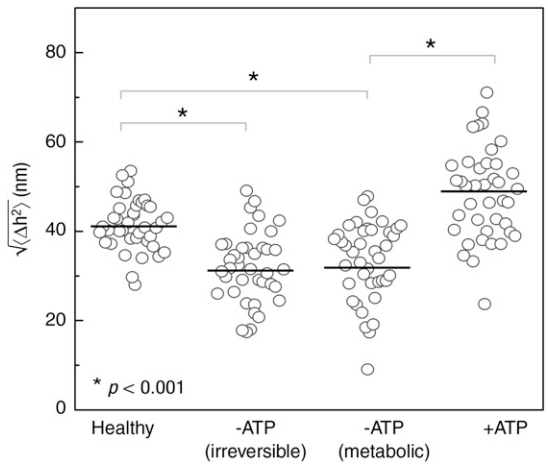

Fig. 2. RMS displacements of membrane fluctuations for different ATP conditions: healthy RBCs, irreversibly ATP-depleted RBCs, metabolically ATP-depleted RBCs, and RBCs in which ATP was reintroduced to metabolically ATP-depleted RBCs. Each *symbol* represents an individual RBC and the *horizontal line* is the mean value.

Even though RBC membrane dynamics have been explored extensively, no definitive experiment has determined whether flickering is purely thermally driven or contains active contributions. First observed a century ago, its origin is generally believed to be thermal forces (2, 16). Different interference-microscopic techniques have been employed to study membrane fluctuations and mechanical properties assuming Brownian dynamics (3, 5). In contrast, a technique that qualitatively measured the local fluctuations of RBC membranes reported a correlation between the ATP concentration and the fluctuation amplitude (9, 10). However, recent experimental work, in which only edge shapes of RBCs were probed, showed no relation between ATP depletion and membrane fluctuations (8). Theoretically, RBC membrane fluctuations were traditionally studied by using models of thermally-driven equilibrium systems (2, 3). A recent

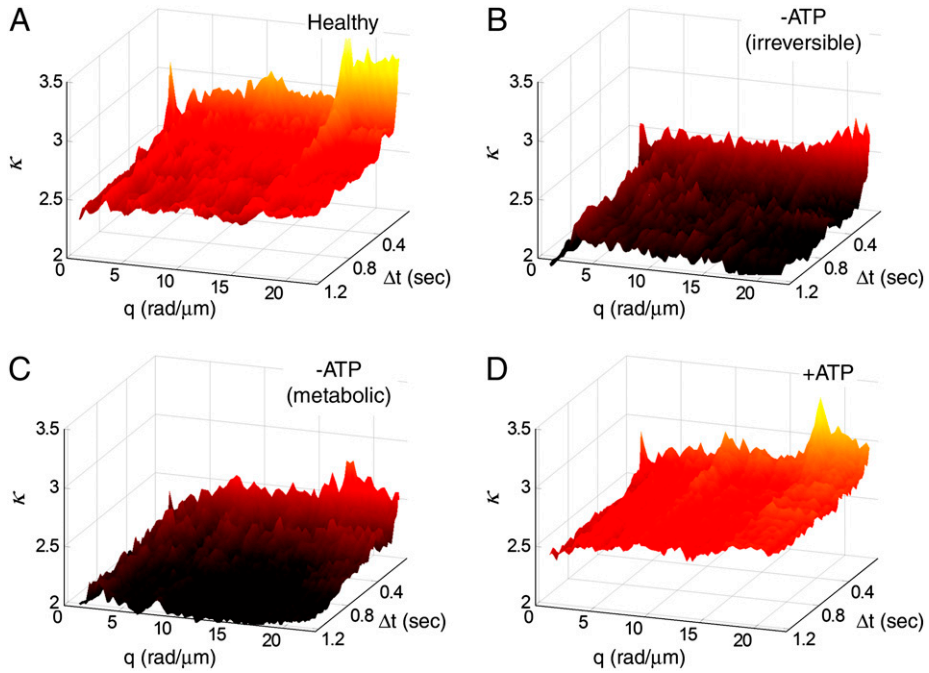

Fig. 3. Non-equilibrium dynamic in RBC membranes. Averaged non-Gaussian parameter, κ, versus a lag time, Δt, and a spatial frequency, q, for membrane fluctuation in healthy RBC, (*A*) irreversible ATP-depletion group, (*B*) metabolic ATP-depletion group, (*C*) and after reintroducing ATP to metabolic-depletion group, (*D*) resp. $N = 40$ RBCs per each group.

theoretical model (15, 17), validated by simulation (18, 19), showed that local breaking and reforming of the spectrin network can result in enhanced fluctuations. Our results here showed that the depletion of ATP decreased the fluctuations in RBC membranes that can be reversed when ATP is reintroduced. Furthermore, measurement of the non-Gaussian parameter κ revealed that the enhanced membrane fluctuations in the presence of ATP are indeed governed by non-equilibrium dynamics, and do not only reflect the change of the mechanical properties of RBCs.

Biconcave Shapes Are Coupled With ATP-Dependent Enhanced Membrane Fluctuations. To study further spatial aspects of active motion, we analyzed the morphologies and fluctuations for RBCs in a polar coordinate system with its origin at cell center. Assuming cylindrical symmetry, the average height of the RBC membrane, $\langle h(r)\rangle$, and the membrane mean-squared displacements, $\langle h^2(r)\rangle$, are shown as functions of the radial distance, r (Fig. 4). In healthy RBCs, the membrane fluctuations are enhanced and strongly localized at the outer convex region (the *shaded area* in Fig. 4), whereas both ATP depletion groups showed little variation in membrane fluctuations over the cell surface. Remarkably, reintroducing ATP restores not only the biconcave shape, but also enhances the fluctuations in the outer convex area. This is striking because continuum equilibrium models predict a stronger restoring force and a decreased fluctuation amplitude in regions of high membrane curvature (20). Our results show that active contributions are spatially inhomogeneous and correlated with the maintenance of the biconcave shape. This strongly suggests that the RBC membrane cortex, especially the coupling and interaction between a lipid layer and spectrin network, is actively and dynamically remodeled in the presence of ATP. It also rationalizes different mechanistic inferences reported in the literature from prior measurement of membrane fluctuations (7, 8, 10). Probing the edge shape of RBCs alone

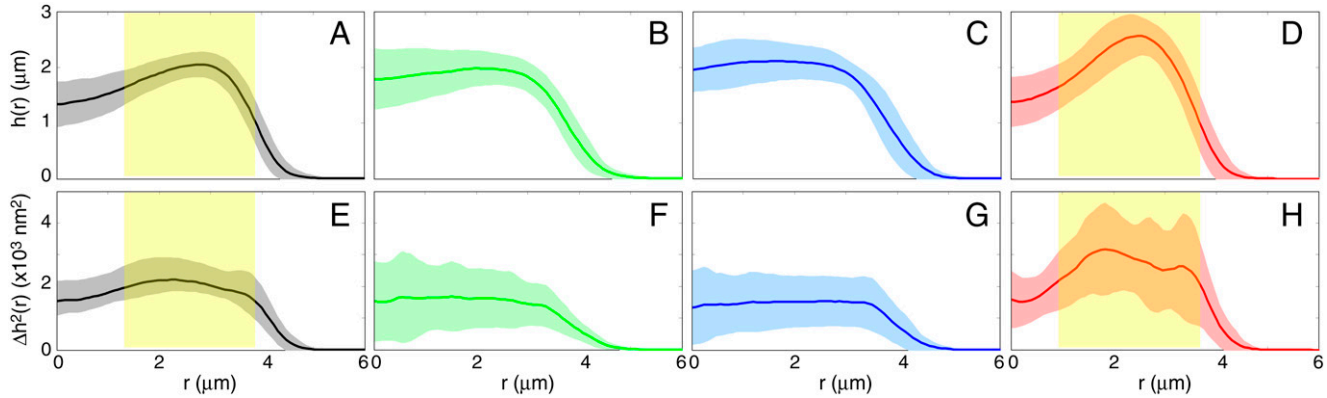

Fig. 4. Correlation between biconcave shape and enhanced membrane fluctuations. (*A–D*) Averaged height as a function of the distance from the center of cells for healthy RBCs, (*A*) for RBCs in the irreversibly ATP-depleted group, (*B*) for RBCs in the metabolically ATP-depleted group, (*C*) and for RBCs in which ATP was reintroduced to the metabolically ATP-depleted group, (*D*) resp. (*E-H*) Averaged squared height fluctuations as a function of the distance from the center of cells in Fig. 3*A–D*, resp. *Thick lines* show the average value and the areas represent standard deviation for 40 RBCs.

does not capture ATP-dependent enhanced fluctuations (8) because they are localized on the convex region on RBC membrane and may not be significant only after 1 h of ATP depletion. Point measurement techniques that measure the averaged dynamics of the RBC membrane could measure ATP-dependence (7, 9, 10).

Spatial Analysis of Membrane Fluctuations. Other cytoskeletons that contain actin, microtubules, and motor proteins such as myosin have demonstrated active motion (21). However, this cannot be the case for the ATP-enhanced fluctuations in RBC because motor proteins are absent here. How can the RBC exhibit active dynamics? To address this question we further analyzed the results in the context of RBC cytoskeletal structure. The non-Gaussian parameter, κ, at short time delays, was plotted as a function of spatial distance $\Lambda = 2\pi/q$ (Fig. 5*A*). Interestingly, in the presence of ATP, κ showed distinct peaks at specific distances ($\Lambda = 361$, 512, 680, 860, and 1030 nm). These peaks are equally spaced at 167 ± 10 nm, which indicates that ATP-dependent enhanced fluctuations are correlated with the network structure of the underlying cytoskeleton. Considering the roughly hexagonal lattice of spectrin network, these peaks can be related to the dynamic remodeling of spectrin network by ATP. Possible elements responsible for this remodeling are the junctional complexes of the spectrin network that join six spectrin polymers by a short, actin segment and protein-4.1 (Fig. 5*B*). It was proposed that the ATP-induced remodeling takes the form of local associations and dissociations of spectrin filaments within the network or between the cytoskeleton and the lipid membrane (4, 15). Both processes result in the formation of a structural defect in the hexagonal network, of size $\sim 2\Delta$, where Δ is a distance between neighboring junctions (Fig. 5*C*). This remodeling of the cytoskeletal attachment causes a local release of the cytoskeleton-induced membrane tension, and results in local bilayer deformation (4, 15). The length scale of this local, ATP-induced bilayer deformation is therefore a multiple of the junction spacing, 2Δ. From the data we find $\Delta \sim 83.5 \pm 5$ nm, which is in good agreement with the separation of the junctions complexes measured by electron microscopy (22). In addition, κ at the short distance 2Δ was plotted as a function of a lag time (Fig. 5*D*) that shows longer temporal correlations in the presence of ATP.

Origin of the Enhanced Fluctuations. The question then arises: how can ATP cause this dynamic remodeling of the cytoskeletal attachment? This may be related to protein phosphorylation powered by ATP that is one of the physiological processes that control membrane stability. One possible candidate is the phosphorylation of the phosphoinositides (PI) because it consumes more ATP than the combined phosphorylation of all the membrane proteins (23). PIP_2, phosphorylated from PI by ATP, is thought to play an important role in modulating the binding of the lipid bilayer to the cytoskeleton by altering the protein interactions that comprise the junctional complex at spectrin tetramer ends (24). For example, PIP_2 strengthens the binding affinity of protein-4.1 to glycophorin C (GP) (25) (Fig. 5*E*). Furthermore, PIP_2 dephosphorylation results in a decreased affinity for GP binding, and a subsequent detachment from spectrin network; the latter can result in increased membrane fluctuations because tension applied to the bilayer by spectrin network is locally and transiently released. In the absence of ATP, this dynamic remodeling may not occur, and thus RBCs exhibit only thermally-driven membrane fluctuations. Another possibility is the phosphorylation of protein-4.1 that results in a reduced binding affinity between the actin, protein-4.1, and GP at the junction (26) (Fig. 5*F*).

Concluding Remarks

The phosphorylation-dependent binding of the cytoskeleton to the membrane can explain the correlation between non-equilibrium dynamic fluctuations and biconcave shape. Several models have

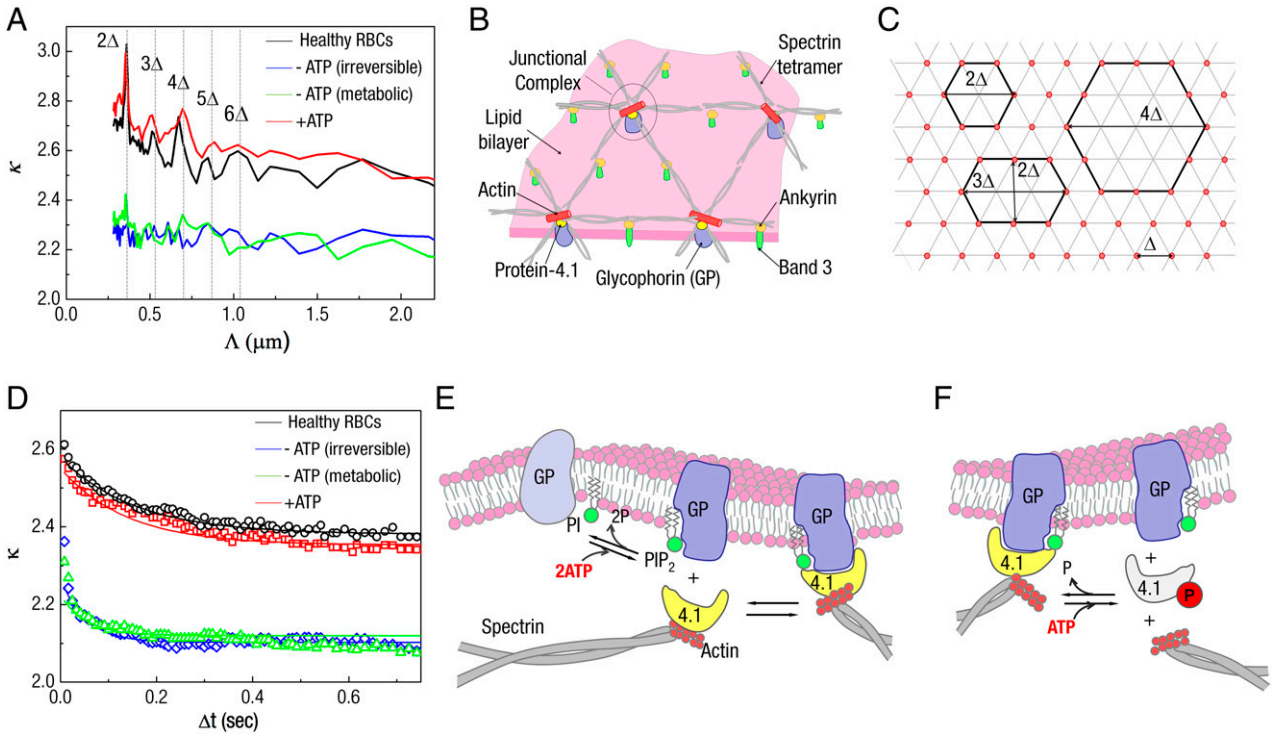

Fig. 5. Cytoskeletal structure and enhanced fluctuations. (*A*) Non-Gaussian parameter at short time delay ($\Delta t < 0.1$ sec) as a function of spatial wavelength. The presence of ATP lead to non-thermal fluctuations, especially at $\Lambda = 361$, 512, 680, 860, and 1030 nm. (*B*) Illustration showing the major proteins in the anchor complexes and the spectrin network. (*C*) Illustration showing the hexagonal lattice of spectrin network and a distance between neighboring junctions, Δ. (*D*) Non-Gaussian parameter at spatial wavelength ($q = 15$ rad/μm) as a function of a lag time. (*E*–*F*) Models explaining the non-equilibrium dynamics in RBC membranes by phosphorylation of PI (*E*) and by phosphorylation of protein-4.1 (*F*).

been proposed to explain the biconcave shape of RBC (27) but it still remains as an unsolved puzzle. It was proposed that the ATP-regulated interaction between the junction complexes and the membrane plays a role in maintaining the biconcave shape (25). A theoretical model that relates ATP-induced unbinding to RBC shape showed that this active process lowers the overall cytoskeleton shear rigidity and the tension that the spectrin network imposes on the membrane (15, 17). Our results provide further experimental evidence for the metabolism-dependent shape transformation. We show that ATP-dependent transient binding of junctional complexes are localized over the cell outer area, and that the spectrin network should therefore exert a lower tension on the membrane. We also note that, in the absence of ATP, the shapes of RBC are similar to those of patients with hereditary elliptocytosis, where GP does not properly interact with protein 4.1, resulting in the lack of biconcave shape and deformability (28, 29). This dynamic remodeling of the spectrin network offers a possible explanation for the observed metabolic dependence of red cell deformability (30). Taken together, we have shown that the biconcave shape and non-equilibrium dynamics in the membrane are both consequences of the same biochemical activity: the dissociations of the cytoskeleton at the spectrin junctions powered by ATP metabolism.

In summary, we have presented definitive evidence that membrane fluctuations in the RBC membrane have a metabolic as well as thermal energy component that are localized at the outer area of the cell. Our results suggest that the spectrin-bilayer binding, through local remodeling of the spectrin junctions, gives rise to this non-equilibrium dynamics. This remodeling is also important in determining cell deformability and the unique biconcave shape of RBCs. Our results are in good qualitative agreement with previously proposed theoretical models (15, 17). The values measured for the ATP-mediated fluctuation amplitudes, which are lower than those predicted theoretically, can be understood by the spatial inhomogeneity of active motions. Whether this dynamic remodeling of the RBC cytoskeleton is beneficial in physiological conditions remains an open question and is now accessible to direct experimental study.

Materials and Methods

Diffraction Phase Microscopy. An Ar^{2+} laser ($\lambda = 514$ nm) was used as illumination source for an inverted microscope (IX71, Olympus). The microscope was equipped with a $40\times$ objective lens (0.75 NA) that facilitates a diffraction-limited transverse resolution of about 400 nm. With the additional relay optics used outside the microscope, the overall magnification of the system was approximately 200×. An Electron Multiplying Charge Coupled Device (Photonmax 512B, Princeton Instruments, Inc.) was used to image interferogram. DPM employs the principle of laser interferometry in a common path geometry and, thus, provides full-field quantitative phase images of RBCs with unprecedented optical path-length stability (11, 12). The instantaneous cell thickness map is obtained as $h(x, y, t) = (\lambda/2\pi\Delta n)\Delta\varphi(x, y, t)$ with $\Delta\varphi$ being the quantitative phase image measured by DPM. The refractive index contrast Δn between the RBC and the surrounding PBS mainly originated from hemoglobin protein that is optically homogeneous in cytosol. We used the Δn of red blood cells calibrated from Tomographic Phase Microscopy (31). The DPM optical path-length stability is 2.4 mrad, which corresponds to a membrane displacement of 3.3 nm (11).

Sample Preparation. Human RBCs were collected in vacutainer tubes containing EDTA, and then immediately centrifuged at $2000 \times g$ for 10 min at 10 °C to separate RBCs from the plasma. The RBCs were washed three times with PBS. For the irreversibly ATP-depleted group, RBCs were incubated without glucose, in the presence of 5 mM inosine (A3221, Sigma–Aldrich) and 3 mM iodoacetamide (I1024, Sigma–Aldrich) for 2 h at 20 °C. Inosine consumes ATP and iodoacetamide blocks ATP production by inhibiting glyceraldehydes-3phosdehydrogenase. For metabolically ATP-depleted group, healthy RBCs were incubated in glucose-free PBS for 24 h at 37 °C. For the ATP-repleted group, 10 mM of D-glucose was added to the RBC suspension in metabolic -ATP group. D-glucose is transported into RBC cytosol and converted into ATP via glycolytic pathways.

Non-Gaussian Parameter. The non-Gaussian parameter, κ, is defined by the second and fourth moments of the membrane height displacement. First, the displacement maps of membrane fluctuations, $\Delta h(x, y, t)$, were decomposed into Fourier modes $\Delta h(q, \Delta t)$. The lag time is Δt and the spatial frequeny, $q = 2\pi/\Lambda$, where Λ is a spatial distance. The non-Gaussian parameter is then calculated from the second and forth moments of the membrane height displacement as $\kappa = \langle|h(q, \Delta t) - h(q, 0)|^4\rangle/\langle|h(q, \Delta t) - h(q, 0)|^2\rangle^2 = \langle|h_q|^4\rangle/\langle|h_q|^2\rangle^2$. When h_q is defined as $h_q = a_q + ib_q$, $\langle a_q^2\rangle = \langle b_q^2\rangle = \frac{1}{2}\langle|h_q|^2\rangle$ and $\langle a_q^4\rangle = \langle b_q^4\rangle = \frac{3}{8}\langle|h_q|^4\rangle$ (14). For Δt longer than the relaxation time of the membrane, the difference of two normally distributed variables is also normally distributed, $\kappa = \langle|h_q|^4\rangle/\langle|h_q|^2\rangle^2 = \frac{8}{3}3/4 = 2$.

Statistical Analysis. *P* values are calculated by two-tailed Mann_Whitney rank sum tests comparing the RMS fluctuations between various test conditions. All the numbers follow the ± sign in the text is a standard deviation.

ACKNOWLEDGMENTS. This research was supported by the National Institutes of Health (P41-RR02594-18). Y.P. has been supported by Samsung Scholarship, and Whitaker Health Science Fellowship. T.A. acknowledges support from the Minerva Foundation. N.S.G. acknowledges support from the Binational Science Foundation (Grant 2006285). S.A.S. acknowledges support from the U.S.-Israel Binational Science Foundation and the Israel Science Foundation. S.S. acknowledges support from the Interdisciplinary Research Group on Infectious Diseases, which is funded by the Singapore-MIT Alliance for Research and Technology Center and from the National Institutes of Health (Grants R01 HL094270-01A1 and 1-R01-GM076689-01). G.P. acknowledges support from National Science Foundation (CAREER: 08-46660).

1. Mohandas N, Evans E (1994) Mechanical properties of the red cell membrane in relation to molecular structure and genetic defects. *Ann Rev Bioph Biom*, 23(1):787–818.
2. Brochard F, Lennon JF (1975) Frequency spectrum of the flicker phenomenon in erythrocytes. *J Phys-Paris*, 36:1035–1047.
3. Zilker A, Engelhardt H, Sackmann E (1987) Dynamic reflection interference contrast (RIC-) microscopy: Anew method to study surface excitations of cells and to measure membrane bending elastic moduli. *J Phys-Paris*, 48:2139–2151.
4. Gov N, Zilman AG, Safran S (2003) Cytoskeleton confinement and tension of red blood cell membranes. *Phys Rev Lett*, 90(22):228101–228104.
5. Popescu G, et al. (2006) Optical measurement of cell membrane tension. *Phys Rev Lett*, 97(21):218101–218104.
6. Popescu G, Park YK, Dasari RR, Badizadegan K, Feld MS (2007) Coherence properties of red blood cell membrane motions. *Phys Rev E*, 76(3):31902–31905.
7. Tuvia S, et al. (1997) Cell membrane fluctuations are regulated by medium macroviscosity: Evidence for a metabolic driving force. *P Natl Acad Sci USA*, 94(10):5045–5049.
8. Evans J, Gratzer W, Mohandas N, Parker K, Sleep J (2008) Fluctuations of the red blood cell membrane: Relation to mechanical properties and lack of ATP dependence. *Biophys J*, 94(10):4134–4144.
9. Betz T, Lenz M, Joanny J, Sykes C (2009) ATP-dependent mechanics of red blood cells. *P Natl Acad Sci USA*, 106(36):15312–15317.
10. Tuvia S, Levin S, Bitler A, Korenstein R (1998) Mechanical fluctuations of the membrane-skeleton are dependent on F-actin ATPase in human erythrocytes. *J Cell Biol*, 141(7):1551–1561.
11. Park YK, Popescu G, Badizadegan K, Dasari RR, Feld MS (2006) Diffraction phase and fluorescence microscopy. *Opt Express*, 14(18):8263–8268.
12. Popescu G, Ikeda T, Dasari RR, Feld MS (2006) Diffraction phase microscopy for quantifying cell structure and dynamics. *Opt Lett*, 31(6):775–777.
13. Sheetz M, Singer S (1977) On the mechanism of ATP-induced shape changes in human erythrocyte membranes. I. The role of the spectrin complex. *J Cell Biol*, 73(3):638–646.
14. Lawrence C, Gov N, Brown F (2006) Nonequilibrium membrane fluctuations driven by active proteins. *J Chem Phys*, 124:074903–074915.
15. Gov NS, Safran SA (2005) Red blood cell membrane fluctuations and shape controlled by ATP-induced cytoskeletal defects. *Biophys J*, 88(3):1859–1874.
16. Parpart A, Hoffman J (1956) Flicker in erythrocytes. "Vibratory movements in the cytoplasm?". *J Cell Compar Physl*, 47(2):295–303.
17. Gov NS (2007) Active elastic network: Cytoskeleton of the red blood cell. *Phys Rev E*, 75 (1):11921–11926.
18. Li J, Lykotrafitis G, Dao M, Suresh S (2007) Cytoskeletal dynamics of human erythrocyte. *P Natl Acad Sci USA*, 104(12):4937–4942.
19. Zhang R, Brown F (2008) Cytoskeleton mediated effective elastic properties of model red blood cell membranes. *J Chem Phys*, 129:065101–065114.
20. Auth T, Safran S, Gov N (2007) Fluctuations of coupled fluid and solid membranes with application to red blood cells. *Phys Rev E*, 76(5):51910–51918.
21. Mizuno D, Tardin C, Schmidt C, MacKintosh F (2007) Nonequilibrium mechanics of active cytoskeletal networks. *Science*, 315(5810):370–373.
22. Liu F, Mizukami H, Sarnaik S, Ostafin A (2005) Calcium-dependent human erythrocyte cytoskeleton stability analysis through atomic force microscopy. *J Struct Biol*, 150(2):200–210.
23. Muller E, et al. (1986) Turnover of phosphomonoester groups and compartmentation of polyphosphoinositides in human erythrocytes. *Biochem J*, 235(3):775–783.

24. Patel V, Fairbanks G (1981) Spectrin phosphorylation and shape change of human erythrocyte ghosts. *J Cell Biol*, 88(2):430–440.
25. Agre P, Parker J (1989) *Red blood cell membranes: structure, function, clinical implications* (CRC Press, New York).
26. Manno S, Takakuwa Y, Mohandas N (2005) Modulation of erythrocyte membrane mechanical function by protein 4.1 phosphorylation. *J Biol Chem*, 280(9):7581–7587.
27. Beutler E (1995) *Williams hematology* (McGraw-Hill, New York), Ch. 22.
28. Tchernia G, Mohandas N, Shohet S (1981) Deficiency of skeletal membrane protein band 4.1 in homozygous hereditary elliptocytosis. Implications for erythrocyte membrane stability. *J Clin Invest*, 68(2):454–460.
29. Weed R, LaCelle P, Merrill E (2006) Mechanical response of human red blood cells in health and disease: Some structure-property-function relationships. *J Mater Res*, 21 (8):1872–1877.
30. Fred M, Pickens M (1969) Metabolic dependence of red cell deformability. *J Clin Invest*, 48(5):795–809.
31. Park Y-K, et al. (2008) Refractive index maps and membrane dynamics of human red blood cells parasitized by Plasmodium falciparum. *P Natl Acad Sci USA*, 105(37):13730–13735.

Supporting Information

Park et al. 10.1073/pnas.0910785107

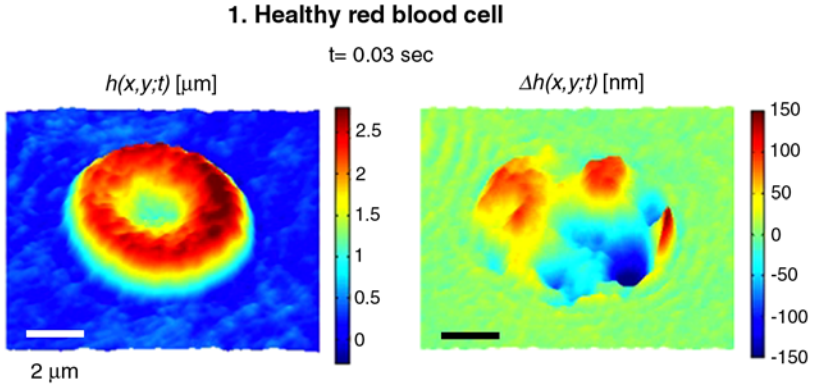

Movie S1. Height map (*Left*) and displacement map (*Right*) of a healthy red blood cell during a 1.3-sec time course (sampling rate is 120 frame/sec).
Movie S1 (MOV)

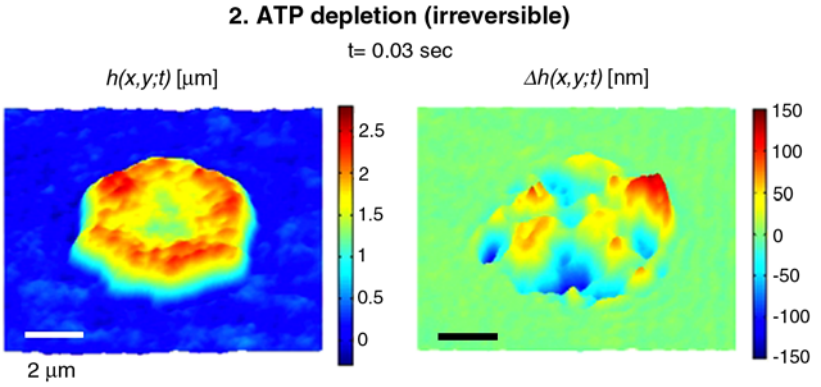

Movie S2. Height map (*Left*) and displacement map (*Right*) of a red blood cell in which ATP is depleted by inosine and iodoacetamide.
Movie S2 (MOV)

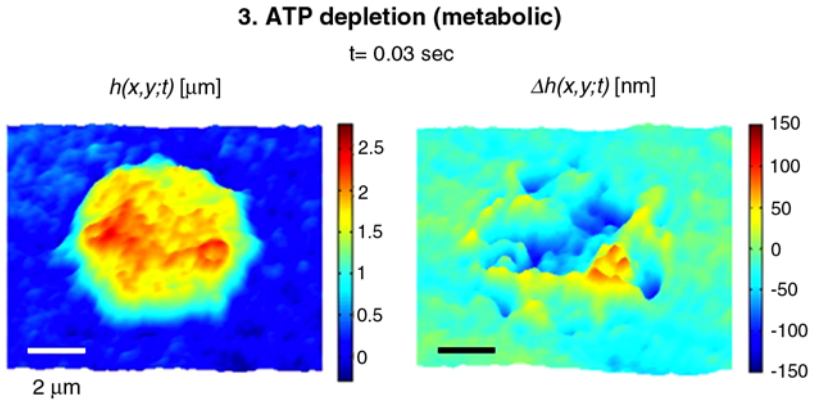

Movie S3. Height map (*Left*) and displacement map (*Right*) of a red blood cell that was incubated in glucose-free medium for 24 hrs for depleting ATP.
Movie S3 (MOV)

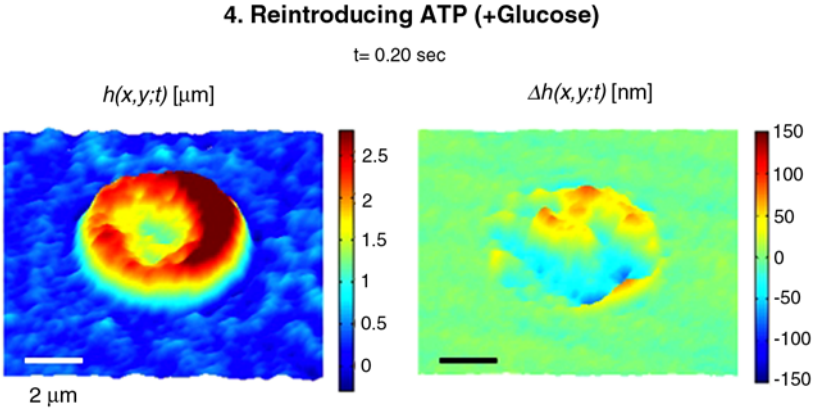

Movie S4. Height map (*Left*) and displacement map (*Right*) of a red blood cell where ATP was first metabolically depleted and then reintroduced by adding glucose.
Movie S4 (MOV)